RSC Advances

This is an *Accepted Manuscript*, which has been through the Royal Society of Chemistry peer review process and has been accepted for publication.

Accepted Manuscripts are published online shortly after acceptance, before technical editing, formatting and proof reading. Using this free service, authors can make their results available to the community, in citable form, before we publish the edited article. This *Accepted Manuscript* will be replaced by the edited, formatted and paginated article as soon as this is available.

You can find more information about *Accepted Manuscripts* in the **Information for Authors**.

Lightweight flexible polyurethane/reduced ultralarge graphene oxide composite foams for electromagnetic interference shielding

Jaber Nasrollah Gavgani[1], Hossein Adelnia[2], Davood Zaarei∗[3], Mohsen Moazzami Gudarzi[*4]

[1]Department of Polymer Engineering and Color Technology, Amirkabir University of Technology, P.O. Box 15875-4413, Tehran, Iran

[2]Young Researchers and Elite Club, Shahreza Branch, Islamic Azad University, P.O. Box: 86145-311, Shahreza, Iran

[3]Department of Polymer Engineering, Technical Faculty, South Tehran Branch, Islamic Azad University, P.O. Box 11365-4435, Tehran, Iran

[4]Department of Inorganic and Analytical Chemistry, School of Chemistry and Biochemistry, University of Geneva, Geneva, Switzerland

---

∗ Corresponding authors: Email: d_zarei@azad.ac.ir; Tel: 982188830326
Email: mohsen.moazzami@unige.ch

Abstract:

Multifunctional flexible polyurethane (PU)/reduced ultralarge graphene oxide (rUL-GO) composite foams with low density in the range of ~53-92 kg/m^3 were fabricated through in-situ polymerization of PU in the presence of rUL-GO. The incorporation of 1 wt% rUL-GOs gave the insular flexible PU composite foams high electrical conductivity of 4.04 S/m, and excellent electromagnetic interference (EMI) shielding efficiency of ~253 dB/(g.cm^{-3}) at 8-12 GHz. Achieving such high specific EMI shielding efficiency as well as low percolation threshold roots in uniform dispersion, very high aspect ratio (> 20000) of rUL-GO nanosheets, combined with the method of foam preparation. Furthermore, by the introduction of rUL-GO, Young's modulus and tensile strength of PU composite foams also improved significantly without scarifying flexibility. TGA experiments also indicated the enhanced thermal stability of the composite foams.

Keywords: Reduced ultra large graphene oxide, Polyurethane foam, EMI shielding, Electrical conductivity

1. Introduction

Optimum design of polymer composite materials is the crucial step to their practical application of these classes of hybrid materials. The core idea of mixing two or more component together is profiting from the right properties of each component and healing the dysfunctionalities of polymeric matrix. Therefore, the most favorable design depends very much on final use of the composite materials. When it comes to use polymeric materials in electromagnetic interference (EMI) shielding, the main disadvantage of common polymers is their electrical insulating nature. Increasing the bulk electrical conductivity of polymer composites to order of 1-10 $S.cm^{-1}$ is often mandatory to achieve suitable and effective EMI shielding.

A common practice to make conductive composites with suitable EMI shielding efficiency is to mix polymer matrix with carbonaceous nanoparticles such as carbon black, carbon nanofiber, carbon nanotubes (CNTs), graphene and its derivatives. The carbon fiber/polystyrene (PS) composite containing 15 vol% showed EMI shielding efficiency of 73.9 in the frequency range of 8-12 GHz [1]. The PS/Fe_3O_4/Thermally reduced graphene oxide (TRG) composite indicated the EMI shielding effectiveness of 25-35 dB in the range of 9.8-12.0 GHz with 2.24 vol% TRG [2]. An EMI shielding effectiveness of approximately 32 dB was obtained by the water-borne polyurethane (PU) composite with contents of 5 vol% non-covalent modified graphene nanosheets [3]. Composite sheets consisting of phenolic resin filled with a mixture of 37 wt% reduced graphene oxide (rGO), 12 wt% γ-Fe_2O_3 and 1 wt% carbon fibers showed the EMI shielding effectiveness of 45..26 dB in the frequency range of 8.2-12.4 GHz [4]. The prepared multilayer graphene/EVA composite film into paraffin-based sandwich structures with 350 μm thickness showed 27 dB EMI shielding efficiency with 69 vol% multilayer graphene nanosheets

[5]. The EMI shielding effectiveness of rGO-SiO$_2$ composite containing 20 wt% rGO was found to be 38 dB at 473 K [6]. The highly aligned rGO/epoxy composite with 2 wt% rGO exhibited EMI shielding efficiency of 38 dB in 0.5-4 GHz [7]. The porous graphene/PS composite containing 5.6 vol% graphene showed EMI shielding effectiveness of 25-30 dB in frequency range of 8-12 GHz [8]. The EMI shielding effectiveness of graphene/polyaniline composite was found to be 34.2 dB at 33 wt% graphene in 8-12 GHz [9]. Yang et al [10] prepared PS/CNT composite foams using a chemical blowing agent. The prepared PS composite foam with 7 wt% CNT exhibited an EMI shielding efficiency of ~20 dB in 8-12 GHz. Zhang et al [11] reported an EMI shielding efficiency of 13-19 dB for polymethylmethacrylate/graphene composite foam with 5 wt% graphene in frequency range of 8-12 GHz. The Graphene-Fe$_3$O$_4$/Polyetherimide (PEI) composite microcellular foam showed an EMI shielding efficiency of 14-18 dB with a Graphene-Fe$_3$O$_4$ loading of 10 wt% in 8-12 GHz [12]. A prepared graphene/poly(dimethyl siloxane) composite foam containing 0.8 wt% graphene indicated 20 dB EMI shielding effectiveness in frequency range of 8-12 GHz [13].

Among them, the latest form, graphene, is attracting great deal of attention not only due to atomically thin nature and extraordinary properties but also because of graphene is more eco-environmentally friendly [14, 15]. Bulk production of graphene and its derivative is now easily possible using wet chemical methods and it is more cost effective than tubular form of carbon. i.e. CNTs. Despite of encouraging results on EMI shielding of graphene-based polymer composites [16], one still wonders if optimal performance of graphenic sheets is obtained or not. Also this is complicated function of different parameters such as level dispersion and alignment, intrinsic properties of graphenic sheets, interaction with polymer matrix and etc. Let's simplify

the problem and just imagine the optimum performance of graphene for increasing electrical conductivity is the initial goal.

Adding graphene (and other conductive fillers) to polymer matrix results in increasing the electrical conductivity if an interconnected network of conductive graphenic sheets forms. As soon as this percolative network forms, electron can pass through the matrix. The threshold that this increase in conductivity happens depends very much on size of graphenic sheets. In fact, the reason this network forms is the excluded volume interaction among them which is due to the 2D nature of them. The larger they are, the higher chance for formation network is. Therefore, it is preferred to use larger graphenic sheets. Another advantage of using large graphenic sheets is lower resistance for passing electron through the composites. There is large resistance at polymer-graphene interface. Using larger sheets substantially decreases the number density of these undesirable resistances too. The remaining challenge is to find effective way of dispersing giant graphenic sheets in polymer matrix.

Light weight PU foams are an excellent candidate as matrix for EMI shielding due to their superior mechanical properties, facile processability, very low density and etc. In this study we used PU as matrix for fabrication of lightweight, conductive and flexible graphene-based composites. Graphene oxide with very high lateral size (few tens of microns, ultra-large graphene oxide, UL-GO) was synthesized according our previous work [17]. Based on a novel method, UL-GO was incorporated in PU matrix and the large size of them was preserved during the processing. In situ polymerization of PU monomers in the presence of rUL-GO was applied to prepare the microcellular PU/rUL-GO composite foams, and rUL-GO with loading up to 1 wt% was added. The properties of PU/rUL-GO composite microcellular foams were investigated in terms of microstructure, electrical conductivity, EMI shielding efficiency, thermal stability,

and mechanical properties. To the best of our knowledge, few studies have investigated the preparation of lightweight microcellular PU composite foams for the application in electrical conducting and EMI shielding fields. This study provides a reproducible and scalable method which may develop the commercialization of such high performance, lightweight, and multifunctional foams.

2. Experimental

2.1 Preparation of reduced ultra large graphene oxide (rUL-GO) nanosheets

UL-GO was synthesized based on the modified Hummers method using expanded graphite [17-20]. The obtained UL-GO nanosheets were diluted by DI water (3 mg/ml) and mildly sonicated for 20 min in a bath sonicator. The UL-GO nanosheets with a mean lateral size of ~ 32.7 μm were obtained. To reduce the UL-GO, hydrazine solution was added to the mixture in the weight ratio of 3:1, while stirring at 80 ºC for 24 h. The mixture was poured into flat molds and dried in an oven at 50 ºC for 6 h to produce rUL-GO nanosheets.

2.2 Preparation of PU/rUL-GO composite foams

The required amounts of the resulting rUL-GOs were mixed with polyether based triol, Voranol 6150 (OH value: 27 mg KOH/g, Dow Plastics) in the reactor. The solution was diluted by high amount of DI water. The reactor was immersed in an oil bath at 100°C. To achieve homogenous dispersion of rUL-GOs, a stirrer along with ultrasonic oscillators was used for 10 h while the water was continuously vaporized. The obtained mixture was dried in an oven at 100 °C for 12 h, and then cooled to room temperature. The prepared mixture (100 phr) along with dibutyltin dilaurate (FASCAT 4202, Arkema Inc.) as a tin catalyst (0.05 phr), TEDA–L33B (33% triethylendiamine in 1,4-butanediol) (0.25 phr), NIAX catalyst E-A-1 (23% bis(2-dimethylaminoethyl) ether in dipropylene glycol) (0.1 phr) as tertiary amine catalysts, the polyol

RSC Advances

based triol, Voranol CP1421 (OH value: 31 mg KOH/g) (4 phr) as a cell-opener, DEOA (85 wt % diethanolamine in water) (0.8 phr) as a crosslink chain extender, SH 209 (0.4 phr) as a silicon surfactant and DI water (2.2 phr) as the blowing agent was mixed with intensive stirring until a uniform mixture was obtained. Then, methylene diphenyl diisocyanate (MDI, Voranate M2940 (NCO content: 31.4 wt %), Dow Plastics) (43.4 phr) was added, and the mixture was stirred for additional 30s. Finally, the mixture was quickly poured into a mold with a lid. The foam expanded and filled the cavities. The obtained foams were post-cured in an oven for 4 h at 100 °C. The abbreviation which will be used for the foams is as PU/rUL-GO*w*: where *w* denotes the weight fraction of loaded rUL-GO. The procedure described above is schematically illustrated in Fig. 1.

Fig. 1 Preparation steps of PU/rUL-GO composite foam

2.3 Characterization

Optical microscopy (OM) was carried out with an optical microscope (ZIESS, Primo Star iLED). Scanning electron microscope (SEM) images of freeze dried UL-GO samples and PU foams were taken by a JEOL-6390 SEM at acceleration voltage of 20 kV. Transmission electron microscope (TEM) was performed with a JEM-2200 FS operating at an accelerating voltage of 200 kV. For TEM investigation, 0.2 mg mL^{-1} of UL-GO dispersion was prepared in DI water by ultra-sonication for 5 min and drop-casted on a fresh carbon TEM grid. X-ray photoelectron spectroscopy (XPS) measurements of the powder samples were performed with an Omicron ESCA Probe (Omicron Nanotechnology, Taunusstein, Germany) using monochromatic Al-K$_\alpha$ radiation (hυ = 1486.6 eV). The X-ray diffraction (XRD) measurements were performed using a Philips1825 with Cu Ka radiation (λ=0.154 nm), operating at 40 keV and with a cathode current of 20 mA. The layer-to-layer distance (d-spacing) of graphite flacks, UL-GO, and rUL-GO

samples is calculated according to Bragg's law; d = nλ/2sinθ, where n is an integer determined by the given order, and λ is the wavelength. Raman spectroscopy (Renishaw MicroRaman/Photoluminescence System) was used to analyze the samples using a 514 nm He-Ne laser. Fourier transform infrared spectra (FTIR) of the samples were obtained using an Equinox 25 Bruker (Canada). The volume conductivity of the moderately conductive samples (> 1×10^{-6} S/m) was measured using a standard four-probe method on a Physical Property Measurement System (Quantum Design, US). The samples with low volume conductivities ($<1\times10^{-6}$ S/m) were measured with a three-terminal fixture on an EST121 ultrahigh resistance and micro current meter (Beijing EST Science & Technology CO. Ltd.). Circular plates with 7 cm in diameter were fabricated for conductivity measurements. The sample surfaces were coated with silver paste to reduce contact resistance between the sample and the electrodes. The EMI shielding property was measured using a WILTRON 54169A scalar measurement system in the frequency range of 8−12 GHz at room temperature. The samples were cut into rectangle plates with a dimension of 22.5×10.0 mm^2 to fit the waveguide sample holder. The thickness of samples was about 2.5 mm. The tensile properties were measured on an Instron 5567 testing machine at a crosshead speed of 2.8 mm/min. At least three specimens were tested for each composition and mean values were reported. The porosity of foams were estimated by the following equation P =1 - $\frac{\rho_{app}}{\rho_{solid}}$,where P is porosity, ρ_{app} is the apparent density determined from the measured mass and volume of PU foam with known size, and ρ_{solid} is the density of solid polyurethane foam and is equal to 1200 kg/m^3 [21]. Thermogravimetric analysis (TGA) was performed on a TGA Q500, TA Analysis, under nitrogen environment at a heating rate of 10 °C/min over a temperature range of 25–600 °C.

3. Results and Discussion

3.1 Characterization of the UL-GO nanosheets

Figure 2a shows OM micrograph of the prepared UL-GO nanosheets confirming a lateral size of tens of micrometers. The corresponding SEM micrograph presented in Fig. 2b further supports the OM micrograph observation. As can be seen, the UL-GO nanosheets mainly have a lateral size of more than 20 μm, while some of them are even between 70-100 μm. However, a few smaller GO nanosheets with the diameter in the range of 5–10 μm are also observed, which is due to breakages of GO nanosheets during the exfoliation process [17, 20]. Moreover, in both OM and SEM formation of single layered GO can be confirmed from homogeneity in contrast of GO sheets on Si/SiO$_2$ substrate [22-24]. However, exfoliation of GO down to single layer is also confirmed using TEM. Figure 2c shows the TEM micrograph of the exfoliated monolayer UL-GO nanosheets. The TEM image indicates that the UL-GO nanosheets are made up of single layers, which is in accordance with the OM, and SEM observations. These observations suggest the exfoliated monolayer UL-GO nanosheets are obtained.

Fig. 2 (a) OM, (b) SEM of UL-GO depositing on Si/SiO$_2$ substrate and (c) TEM micrographs of the as-produced UL-GO nanosheets.

Figure 3 shows the XRD patterns of the natural graphite flakes, UL-GO, and rUL-GO samples. A sharp reflection $2\theta = 26.5°$ in the XRD scattering pattern of pristine graphite originates from the interlayer (002) spacing (d-spacing = 0.337 nm). Upon oxidation, neighboring layers are $\sim$ 0.87 nm apart ($2\theta = 10.1°$) because of the intercalation by oxygen groups and moisture. Moreover, in case of UL-GO, peak broadening and the shift to lower angle takes place owning to the disorder introduced by reduced average crystalline size. For the rUL-GO, characteristic reflections are absent, implying high exfoliation via chemical reduction of UL-GO [17, 25].

Fig. 3 XRD patterns of (a) natural graphite flakes, (b) UL-GO, and (c) rUL-GO samples. The d-spacing is represented by d.

The results from the XPS analysis are shown in Fig. 4. The C1s spectra are compared between the UL-GO and rUL-GO. The spectra were deconvoluted into three peaks corresponding to the following functional groups: carbon sp^2 (C=C and C-C), carbon sp^3, epoxy/hydroxyl (C–O), and carbonyl (C=O), and the summary is presented in Table 1. C1s XPS spectra of UL-GO indicates considerably degree of oxidation that means the presence of different oxygen functional groups in UL-GO structure (e.g. carbonyl, epoxy, hydroxyl groups) [17, 26, 27]. Peaks corresponding to the covalent bonds of carbon and oxygen atoms are more intense for UL-GO than for rUL-GO. Therefore, it can be said that the reduction process was successful in eliminating oxidized carbon in the form of carbonyl and epoxy/hydroxyl groups.

Table 1. Summary of the relative percentages of the carbon and assignation.

Binding energy (eV) and assignation	284.6 eV C-C and C=C	286.6-287.0 eV C-O	287.8-288.2 eV C=O
UL-GO	48.6	44.8	6.6
rUL-GO	70.0	17.5	12.5

Fig. 4 C1s XPS spectra of (a) UL-GO and (b) rUL-GO.

FTIR spectra of UL-GO before and after reduction by hydrazine are shown in Fig. S1. The UL-GO displayed the typical absorption bands at 1717 (carboxyl C=O), 1633 (C=C), 1398 (carboxy C–O), 1225 (epoxy C–O), and 1055 cm^{-1} (alkoxy/alkoxide C–O). Also, a broad band centered at 3437 cm^{-1} was seen in the spectrum which is ascribed to the hydroxyl groups located

on the surface of UL-GO [28]. After the reduction, the intensities of all absorption bands related to the oxygenous groups decreased dramatically, indicating that UL-GO have been almost completely reduced to rUL-GO.

The Raman spectra for the UL-GO and rUL-GO were also characterized as shown in Fig. 5. For both samples, distinctive peaks for the D bands and G bands could be observed. It was observed that the D to G band intensity ratio, I_D/I_G, increased from 0.78 (UL-GO) to 0.83 (rUL-GO) as well as the G peak position red shifted upon reduction to rUL-GO. The decrease in the size of the newly formed graphene-like sp^2 domains is also partly responsible for the increase in the intensity ratio, I_D/I_G [17, 29]. Moreover, a prominent D peak is a reflection of disorder in the carbon structure, the above observations are consistent with previous reports on similar rUL-GO [30, 31].

Fig. 5 Raman spectra of UL-GO and rUL-GO.

3.2 Characterization of PU/rUL-GO composite foams

The dispersion and chemical interaction of rUL-GOs in PU matrix are critical issues in the development of meaningful materials for various applications [32]. Therefore, XRD and FTIR analyses were respectively performed to evaluate dispersion state and chemical interaction of rUL-GO with PU matrix (Figs. 6 and 7). The XRD pattern of PU/rUL-GO1 foam was almost the same as that of pure PU foam, without the presence of graphite or GO layer structure diffraction peak at 26° and 10.1° (Shown in Fig. 6). These results clearly indicate that rUL-GO is fully exfoliated into individual graphene nanosheets in the PU matrix [33, 34]. The XRD patterns of other PU/rUL-GO composite foams also showed the same results (data not shown).

Fig .6 XRD patterns of rUL-GO nanosheet, pure PU, and PU/rUL-GO1 foams.

Figure 7 shows FTIR spectra of pure PU and PU/rUL-GO1 foams. Since the rUL-GO nanosheets derived by chemical synthesis possess remnant oxygenated groups, these active sites may interact with urethane, carboxyl and isocyanate groups of PU chains to form strong interfacial adhesion [18, 35-37]. The pure PU foam showed its characteristic bands at: 3427, and 3520 cm^{-1} (as a shoulder), which are attributed to stretching vibration of hydrogen bonded and free N-H groups, respectively. The absorption bands related to non-symmetric and symmetric stretching vibration of CH_2 were observed at 2930 and 2866 cm^{-1}, respectively. The peaks at 1722, 1228 and 1072 cm^{-1} are attributed to stretching vibration of carbonyl (C=O), the stretching vibration of aromatic C-O, and the non-symmetric stretching vibration of C-O-C, respectively. The combination of N-H deformation and C-N stretching vibrations occurs at 1533 and 1228 cm^{-1}, respectively. By comparing FTIR spectra of pure PU and PU/rUL-GO1 foams, two significant changes are noted. First, the shoulder at 3520 cm^{-1} completely disappeared in PU/rUL-GO1 foam. Second, the peak related to the C=O groups of PU was shifted from 1722 to 1699 cm^{-1}. These results indicate that both free N-H, and C=O groups of PU become involved in hydrogen bonding interactions with the remaining oxygenated groups of rUL-GO nanosheets [35, 37]. Besides, the bands at 1379, 1228, 1072 cm^{-1} completely disappeared after the addition of rUL-GO, further supporting the presence of strong interfacial adhesion and chemical interaction between PU chains and rUL-GO nanosheets.

Fig. 7 FTIR spectra of pure PU and PU/rUL-GO1 foams, the highlighted region in original spectrum is magnified in the right-hand image.

Figure 8 depicts the electrical conductivity of PU composite foams plotted as a function of rUL-GO content. The conductivity of pure PU ($\sim 10^{-11}$ S/cm) is in a good agreement with the values reported in the literature [18]. On the other hand, the conductivity of thermally exfoliated

graphene has been reported to be ~ 80 S/cm [25]. As can be seen, the electrical conductivity of PU

composite foams exponentially increased at low rUL-GO contents, followed by a slow increase

at higher contents. Thanks to the homogenous dispersion of monolayer rUL-GO nanosheets in

the PU matrix, the electrical conductivity was sharply raised by nearly 7 orders of magnitude

when 0.4 wt% rUL-GO was incorporated. Up to 1 wt% of rUL-GO, electrical conductivity

increased with a lower rate, then reached to a plateau. It is noteworthy to mention that the

electrical conductivity of 4.04-9.34 S/m at rUL-GO content in the range of 1-2 wt % was

achieved, making these composite foams very promising to be considered in the electronic

industry, in areas such as electromagnetic interference shielding, electrostatic discharge

protection, actuators and photoconductors.

It should be added that, generally, as the amount of conductive filler gradually increases,

the foam undergoes a rapid insulator-to-conductor transition at certain nanofiller content,

referred to as percolation threshold. The percolation threshold, φ_c, was calculated based on the

power law equation [38, 39]:

$$\sigma_c = \sigma_f(\varphi - \varphi_c)^n \tag{1}$$

where σ_c, σ_f, and φ are the conductivity of composite foam, filler conductivity, and filler

content, respectively. From the log–log plot of the equation, the percolation threshold was

obtained to be $\varphi_c = 0.06$ wt% (shown in the inset of Fig. 8). The percolation threshold value in

terms of volume fraction was obtained to be about 0.029 vol%, by considering the densities of

PU (1.05 g.cm^{-3}) and graphene (2.2 g.cm^{-3}). It should be highlighted that the percolation

threshold values of foams are generally lower than that of their corresponding bulk composites.

For example, Yousefi et al. [39] achieved the percolation threshold of 0.16 wt% in PU bulk

composites using nearly the same size rUL-GO. In general, obtaining the lower percolation threshold value in polymer foams stems from two effects; one is that cell formation followed by in-situ generated strong extensional flow pushes nanosheets together, and considerably facilitates the orientation of nanoparticles in cell wall [40]. The other effect of the foaming process is the volume expansion, which increases the distance of adjacent nanoparticles [41].

To the best of the authors' knowledge, up until now, the obtained percolation threshold value is one of the lowest one reported in the literature not only for polymer/graphene composites foams but also for bulk composites. The lowest percolation threshold values of composite foams filled with graphene for different polymer matrices are summarized as follows; PMMA ($\varphi_c \sim$ 0.66 wt %) [11], polyvinylidene fluoride ($\varphi_c \sim$ 0.5 wt %) [42], and PEI ($\varphi_c \sim$ 0.63 wt %) [41]. The ultralow percolation threshold value obtained in this work is ascribed to the following features of the PU composite foams: first, inherently high electrical conductivity of rUL-GO; second, good state of dispersion; last but not the least, ultralarge size of monolayer graphene nanosheets.

Kim et al [43] proposed an improved analytical model based on the average interparticle distance concept, predicting the percolation threshold of polymer composites filled with nanoplatelets or disk-shaped fillers. According to the results of this model, a percolation threshold of 0.029 vol% is equivalent to an aspect ratio in order of 10^4. Assuming that if all of the rUL-GO nanosheets were exfoliated in the PU matrix as monolayer sheets (i.e., the thickness of about 1 nm), an aspect ratio of 10^4 would be equivalent to the average lateral size of 10 μm. This estimation is in the same of the size of GO sheets used in this study verifying molecular-level dispersion of individual rGO nanosheets in the PU matrix [39]. Lower estimation of aspect ratio compared to what observed experimentally (Fig. 2 and Ref. 17) might be due to mere

breakage of nanosheets, inherent flexibility of them (especially at such high aspect ratio) and also imperfection in dispersion. However, these findings further emphasize the high potential of using rUL-GO nanosheets as highly efficient ECNs for the production of highly electrically conductive materials.

Fig. 8 Electrical conductivity of PU/rUL-GO composite foams as a function of rUL-GO content (wt %); Inset: log σ plotted against log(φ-φ_c).

The EMI shielding of the PU/rUL-GO composite foams with a thickness of 2.5 mm was determined in the microwave frequency range of 8-12 GHz (Fig. 9). The measured shielding efficiency is defined as

$$EMI\ shielding = 10\ log\frac{P_{in}}{P_{out}} \tag{1}$$

where P_{in} is the incident power and P_{out} is the power transmitted through a shielding material, and it is directly related with its conductivity. As shown in Fig. 9a, the EMI shielding of PU/rUL-GO composite foams presented weak frequency dependency at the X-band. The EMI shielding of PU/rUL-GO composite foams increased gradually up to ~23 dB at 1 wt % rUL-GO loading, which indicates that EMI shielding properties of these foams are enhanced with the increase of rUL-GO loading. Figure 9b summarizes the specific EMI shielding of polymer composite foams reported by other researchers [10, 11, 41, 44, 45]. It is worth noting that our PU/rUL-GO composite foam with 1 wt% rUL-GO presented a higher specific EMI shielding than other foaming systems, resulting possibly from the large surface area of as-prepared rUL-GO and he good dispersion of ultralarge size of monolayer graphene nanosheets in cell walls [35, 39, 41]. These results strongly suggest that such microcellular PU/rUL-GO composite foams are very promising

for use as lightweight and high-performance EMI shielding materials with strong microwave absorption.

Fig. 9 (a) EMI shielding efficiency of PU/rUL-GO composite foam at different frequency (b) The comparative of specific EMI shielding efficiency of our data with other reported results.

The mechanical strength of the composite foams is of great importance especially when they are generally exposed to high stress and strain fields. The interfacial interactions, orientation, aspect ratio, and surface functional groups of the nanofiller are some important factors which play a key role in determining the mechanical properties [46-48]. The mechanical properties of pure PU and PU composite foams (Fig. S2) are summarized in Table 2. Even though the changes in mechanical characteristic of the samples were remarkable, they still exhibited their typical elastomeric behavior. Interestingly, as low as 0.1 wt % of rUL-GO increased the Young's modulus and tensile strength from 5.5 to 42.6 MPa and from 15.3 to 30.2 MPa, respectively. The elongation at break of the composite foams was lower than that of pure PU foam, but obtained values are still in the range of the high-elongation-at-break foams. The notable improvement of modulus in PU composite foams is due to the well exfoliated rUL-GO nanosheets as well as strong interfacial bonding between PU chains and rUL-GOs. As demonstrated in FTIR section, the remnant oxygenated functional groups on the surface of rUL-GOs interact with the urethane groups of PU. Such interactions lead to well dispersed and exfoliated monolayer rUL-GO nanosheets, and consequently resulting in a strong interfacial adhesion between PU and nanosheets [18, 37, 49]. However, these interactions increase the molecular restrictions of the PU chains, and in turn decrease the elongation at break of the composite foams as compared to that of the pure PU foam.

Table 2. Mechanical properties, density, and porosity of flexible pure PU and PU/rUL-GO composite foams.

Sample	Tensile strength (MPa)	Young's modulus (MPa)	Density (kg/m^3)	Porosity (%)
Pure PU	15.3 ± 0.05	5 ± 0.1	53 ± 6	95.58 ± 0.50
PU/rUL-GO0.1	30.2 ± 0.06	42.6 ± 0.3	58 ± 5	95.16 ± 0.41
PU/rUL-GO0.5	38.4 ± 0.04	62.9 ± 0.1	72 ± 7	94.00 ± 0.59
PU/rUL-GO1	54.2 ± 0.2	75.2 ± 0.2	92 ± 9	92.33 ± 0.75

The surface morphology of pure PU and PU/rUL-GO1 foams is shown in Fig. 10. The PU foams exhibits 3D-hierarchical mesoporous structure with the pore size ranging from 500 to 1200 μm which results from the high expansion ratio of the foaming. The density of PU composite foams increased with increasing rUL-GO content which is ascribed to an increase of the polyol viscosity [50, 51] (Table 2). The increase in density of PU composites not only decreased the porosity, but also led to a more polyhedrons open cell structures. Despite this porosity reduction, the composite foams are still considered as highly porous materials, and therefore possess good compressibility and large internal surface area. Moreover, smooth inner and outer layers of these polyhedron open cell structures are free from the inter-junctions that enhances superior electrical conducting path.

Fig. 10 SEM micrographs of (a) pure PU, and (c) PU/rUL-GO1 foams. b, and d are the corresponding higher magnification of a and c, respectively.

Thermal stability of the pure PU and PU/rUL-GO1 foams is shown in Fig. 11. It has widely been reported that PU has a three-stage degradation process at 370–400, 400–440, and 470–550 °C. These three characteristic temperatures referred to as T_{1st}, T_{2st}, and T_{3st}, respectively. The first stage is attributed to the dimerization and trimerization reaction of isocyanates [18, 52]; the second step is due to de-polymerization of PU to form isocyanate, the primary or secondary amine, polyol, olefin, and carbon dioxide; and the last degradation step is assigned to the decomposition of hard segment [53, 54]. It is important to note that slight variations, though negligible, seen in thermogram curves of pure PU foam is due to the presence of foaming additive components. Similarly, the typical three-stage degradation process is seen in PU/rUL-GO1 thermogram curve. The effect of the 1wt % rUL-GO on the degradation steps of PU foams, in terms of the characteristic temperatures, is shown on Table 3. The addition of 1 wt % rUL-GO, increases the T_{1st}, T_{2st}, and T_{3st} by about 14, 27, and 37 °C, respectively. Moreover, as can be seen, the addition of 1 wt % rUL-GO improved heat dissipation as well as thermal stability of PU/rUL-GO1 foam as compared to pure PU one. There are several factors responsible for such a conspicuous thermal stability improvement. First, the interaction of the remnant oxygenated functional groups of rUL-GO with urethane groups of PU, mentioned in FTIR section, enhance interfacial adhesion, between PU chains and rUL-GOs [55, 56]. Well dispersed and monolayer exfoliated rUL-GO nanosheets provide high surface for direct covalent bonding with the PU matrix. These results continued to support the conclusion that the rUL-GO nanosheets can act as a barrier to reduce the diffusion of volatile compounds and hence an enhancement of the thermal stability is observed [18].

Fig. 11 TGA trace of pure PU and PU/rUL-GO1 foams under nitrogen atmosphere; Inset: DTG trace.

Table 3. Degradation temperatures of flexible pure PU and PU/rUL-GO1 foams.

Sample	T_{1st}	T_{2st}	T_{3st}
Pure PU foam	382	420	521
PU/rUL-GO1 foam	396	447	557

4. Conclusion

Lightweight flexible PU/rUL-GO composite foams with high electrical conductivity and specific EMI shielding efficiency have been fabricated by in-situ polymerization of PU in the presence of rUL-GO. OM, SEM, and TEM micrographs showed the ultralarge size and monolayer structure of as-prepared GO. Interestingly, thanks to the ultralarge size of rGO nanosheets, the PU composite foams exhibited ultralow percolation concentration of 0.06 wt% and high electrical conductivity of 9.34 S/m with a low rUL-GO loading of 2 wt%, as well as excellent specific EMI shielding efficiency of ~253 in the presence of 1 wt% rUL-GO. In addition, the PU/rUL-GO composite foams exhibited not only improved mechanical properties, but also a good thermal stability. Overall, it has been demonstrated that such flexible conductive PU/rUL-GO composite foams with improved properties can exhibit the potential for use as a novel EMI shielding materials.

Acknowledgements

References

1.   X. Shui and D. Chung, *Journal of electronic materials*, 1997, **26**, 928-934.
2.   Y. Chen, Y. Wang, H.-B. Zhang, X. Li, C.-X. Gui and Z.-Z. Yu, *Carbon*, 2015, **82**, 67-76.

3. S.-T. Hsiao, C.-C. M. Ma, H.-W. Tien, W.-H. Liao, Y.-S. Wang, S.-M. Li and Y.-C. Huang, *Carbon*, 2013, **60**, 57-66.

4. A. P. Singh, P. Garg, F. Alam, K. Singh, R. Mathur, R. Tandon, A. Chandra and S. Dhawan, *Carbon*, 2012, **50**, 3868-3875.

5. W.-L. Song, M.-S. Cao, M.-M. Lu, S. Bi, C.-Y. Wang, J. Liu, J. Yuan and L.-Z. Fan, *Carbon*, 2014, **66**, 67-76.

6. B. Wen, M. Cao, M. Lu, W. Cao, H. Shi, J. Liu, X. Wang, H. Jin, X. Fang and W. Wang, *Advanced Materials*, 2014, **26**, 3484-3489.

7. N. Yousefi, X. Sun, X. Lin, X. Shen, J. Jia, B. Zhang, B. Tang, M. Chan and J. K. Kim, *Advanced Materials*, 2014, **26**, 5480-5487.

8. D.-X. Yan, P.-G. Ren, H. Pang, Q. Fu, M.-B. Yang and Z.-M. Li, *Journal of Materials Chemistry*, 2012, **22**, 18772-18774.

9. B. Yuan, L. Yu, L. Sheng, K. An and X. Zhao, *Journal of Physics D: Applied Physics*, 2012, **45**, 235108.

10. Y. Yang, M. C. Gupta, K. L. Dudley and R. W. Lawrence, *Nano letters*, 2005, **5**, 2131-2134.

11. H.-B. Zhang, Q. Yan, W.-G. Zheng, Z. He and Z.-Z. Yu, *ACS applied materials & interfaces*, 2011, **3**, 918-924.

12. B. Shen, W. Zhai, M. Tao, J. Ling and W. Zheng, *ACS applied materials & interfaces*, 2013, **5**, 11383-11391.

13. Z. Chen, C. Xu, C. Ma, W. Ren and H. M. Cheng, *Advanced materials*, 2013, **25**, 1296-1300.

14. F. Schedin, A. Geim, S. Morozov, E. Hill, P. Blake, M. Katsnelson and K. Novoselov, *Nature materials*, 2007, **6**, 652-655.

15. D. Li, M. B. Müller, S. Gilje, R. B. Kaner and G. G. Wallace, *Nature nanotechnology*, 2008, **3**, 101-105.

16. M.-S. Cao, X.-X. Wang, W.-Q. Cao and J. Yuan, *Journal of Materials Chemistry C*, 2015, **3**, 6589-6599.

17. S. H. Aboutalebi, M. M. Gudarzi, Q. B. Zheng and J. K. Kim, *Advanced Functional Materials*, 2011, **21**, 2978-2988.

18. J. N. Gavgani, H. Adelnia and M. M. Gudarzi, *Journal of Materials Science*, 2014, **49**, 243-254.

19. Q. B. Zheng, M. M. Gudarzi, S. J. Wang, Y. Geng, Z. Li and J.-K. Kim, *Carbon*, 2011, **49**, 2905-2916.

20. M. M. Gudarzi, M. H. M. Moghadam and F. Sharif, *Carbon*, 2013, **64**, 403-415.

21. R. Hodlur and M. Rabinal, *Composites Science and Technology*, 2014, **90**, 160-165.

22. I. Jung, J.-S. Rhyee, J. Y. Son, R. S. Ruoff and K.-Y. Rhee, *Nanotechnology*, 2011, **23**, 025708.

23. J. Kim, F. Kim and J. Huang, *Materials today*, 2010, **13**, 28-38.

24. A. Dimiev, D. V. Kosynkin, A. Sinitskii, A. Slesarev, Z. Sun and J. M. Tour, *Science*, 2011, **331**, 1168-1172.

25. Z.-S. Wu, W. Ren, L. Gao, J. Zhao, Z. Chen, B. Liu, D. Tang, B. Yu, C. Jiang and H.-M. Cheng, *Acs Nano*, 2009, **3**, 411-417.

26. H. J. Shin, K. K. Kim, A. Benayad, S. M. Yoon, H. K. Park, I. S. Jung, M. H. Jin, H. K. Jeong, J. M. Kim and J. Y. Choi, *Advanced Functional Materials*, 2009, **19**, 1987-1992.

27. S. Pei and H.-M. Cheng, *Carbon*, 2012, **50**, 3210-3228.

28. Y. Zhu, M. D. Stoller, W. Cai, A. Velamakanni, R. D. Piner, D. Chen and R. S. Ruoff, *Acs Nano*, 2010, **4**, 1227-1233.

29. D. Yang, A. Velamakanni, G. Bozoklu, S. Park, M. Stoller, R. D. Piner, S. Stankovich, I. Jung, D. A. Field and C. A. Ventrice, *Carbon*, 2009, **47**, 145-152.

30. W. Gao, L. B. Alemany, L. Ci and P. M. Ajayan, *Nature chemistry*, 2009, **1**, 403-408.

31. C. Gómez-Navarro, J. C. Meyer, R. S. Sundaram, A. Chuvilin, S. Kurasch, M. Burghard, K. Kern and U. Kaiser, *Nano letters*, 2010, **10**, 1144-1148.

32.   H. C. Bidsorkhi, H. Adelnia, N. Naderi, N. Moazeni and Z. Mohamad, *Polymer Composites*, 2015.
33.   H. Kim, Y. Miura and C. W. Macosko, *Chemistry of Materials*, 2010, **22**, 3441-3450.
34.   J. Liang, Y. Huang, L. Zhang, Y. Wang, Y. Ma, T. Guo and Y. Chen, *Advanced Functional Materials*, 2009, **19**, 2297-2302.
35.   N. Yousefi, M. M. Gudarzi, Q. Zheng, X. Lin, X. Shen, J. Jia, F. Sharif and J.-K. Kim, *Composites Part A: Applied Science and Manufacturing*, 2013, **49**, 42-50.
36.   J. N. Gavgani, H. Adelnia, G. Mir Mohamad Sadeghi and F. Zafari, *Journal of Applied Polymer Science*, 2014, **131**.
37.   Y. C. Jung, J. H. Kim, T. Hayashi, Y. A. Kim, M. Endo, M. Terrones and M. S. Dresselhaus, *Macromolecular rapid communications*, 2012, **33**, 628-634.
38.   S. Kirkpatrick, *Reviews of modern physics*, 1973, **45**, 574.
39.   N. Yousefi, M. M. Gudarzi, Q. Zheng, S. H. Aboutalebi, F. Sharif and J.-K. Kim, *Journal of Materials Chemistry*, 2012, **22**, 12709-12717.
40.   W. Zhai, J. Wang, N. Chen, H. E. Naguib and C. B. Park, *Polymer Engineering & Science*, 2012, **52**, 2078-2089.
41.   J. Ling, W. Zhai, W. Feng, B. Shen, J. Zhang and W. g. Zheng, *ACS applied materials & interfaces*, 2013, **5**, 2677-2684.
42.   V. Eswaraiah, V. Sankaranarayanan and S. Ramaprabhu, *Macromolecular Materials and Engineering*, 2011, **296**, 894-898.
43.   J. Li and J.-K. Kim, *Composites science and technology*, 2007, **67**, 2114-2120.
44.   J. Liang, Y. Wang, Y. Huang, Y. Ma, Z. Liu, J. Cai, C. Zhang, H. Gao and Y. Chen, *Carbon*, 2009, **47**, 922-925.
45.   Y. Yang, M. C. Gupta, K. L. Dudley and R. W. Lawrence, *Journal of nanoscience and nanotechnology*, 2005, **5**, 927-931.
46.   S. Rana, J. W. Cho and L. P. Tan, *RSC Advances*, 2013, **3**, 13796-13803.
47.   H. Adelnia, H. C. Bidsorkhi, A. Ismail and T. Matsuura, *Separation and Purification Technology*, 2015, **146**, 351-357.
48.   H. C. Bidsorkhi, H. Adelnia, R. H. Pour and M. Soheilmoghaddam, *Journal of Materials Science*, 2015, **50**, 3237-3245.
49.   C. Wu, X. Huang, G. Wang, X. Wu, K. Yang, S. Li and P. Jiang, *Journal of Materials Chemistry*, 2012, **22**, 7010-7019.
50.   M. M. Bernal, I. Molenberg, S. Estravis, M. A. Rodriguez-Perez, I. Huynen, M. A. Lopez-Manchado and R. Verdejo, *Journal of Materials Science*, 2012, **47**, 5673-5679.
51.   R. Verdejo, R. Stämpfli, M. Alvarez-Lainez, S. Mourad, M. Rodriguez-Perez, P. Brühwiler and M. Shaffer, *Composites Science and Technology*, 2009, **69**, 1564-1569.
52.   M. Luda, P. Nada, L. Costa, P. Bracco and S. Levchik, *Polymer degradation and stability*, 2004, **86**, 33-41.
53.   M. Ravey and E. M. Pearce, *Journal of Applied Polymer Science*, 1997, **63**, 47-74.
54.   D. Chattopadhyay and D. C. Webster, *Progress in Polymer Science*, 2009, **34**, 1068-1133.
55.   X. Wang, Y. Hu, L. Song, H. Yang, W. Xing and H. Lu, *J. Mater. Chem.*, 2011, **21**, 4222-4227.
56.   T. Ramanathan, A. Abdala, S. Stankovich, D. Dikin, M. Herrera-Alonso, R. Piner, D. Adamson, H. Schniepp, X. Chen and R. Ruoff, *Nature nanotechnology*, 2008, **3**, 327-331.
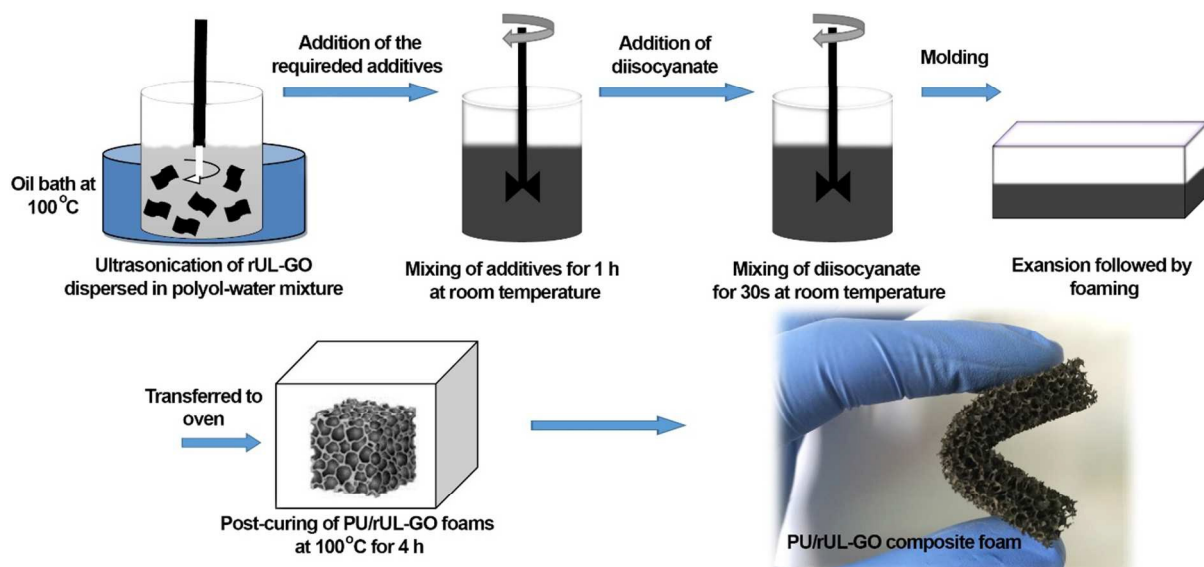
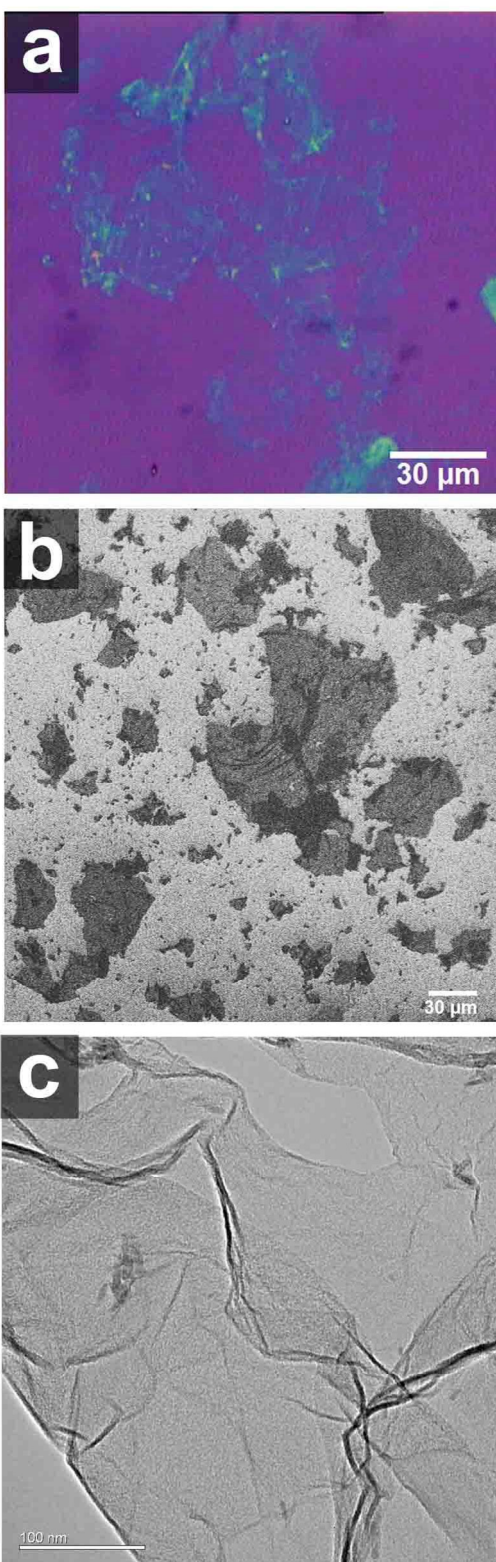Fig. 1 Preparation steps of PU/rUL-GO composite foam

Fig. 2 (a) OM, (b) SEM of UL-GO depositing on Si/SiO$_2$ substrate and (c) TEM micrographs of the as-produced UL-GO nanosheets.
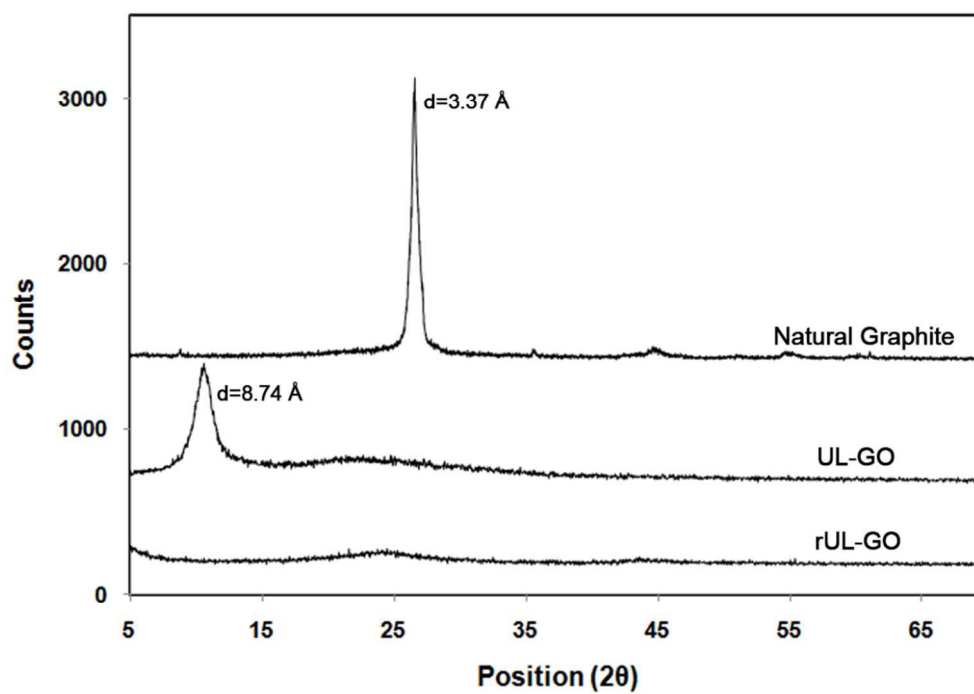
Fig .3 XRD patterns of (a) natural graphite flakes, (b) UL-GO, and (c) rUL-GO samples. The d-
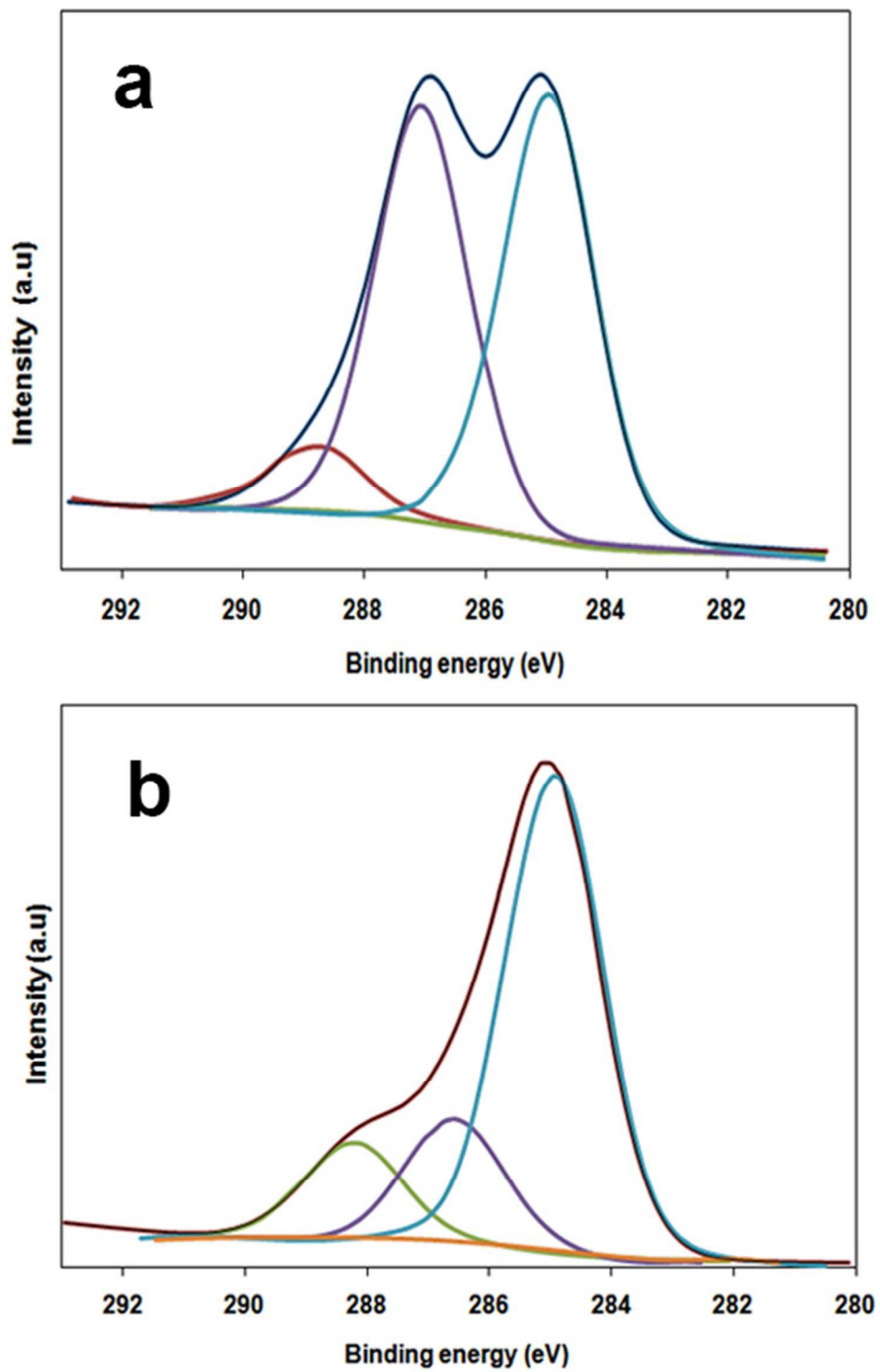
spacing is represented by d.

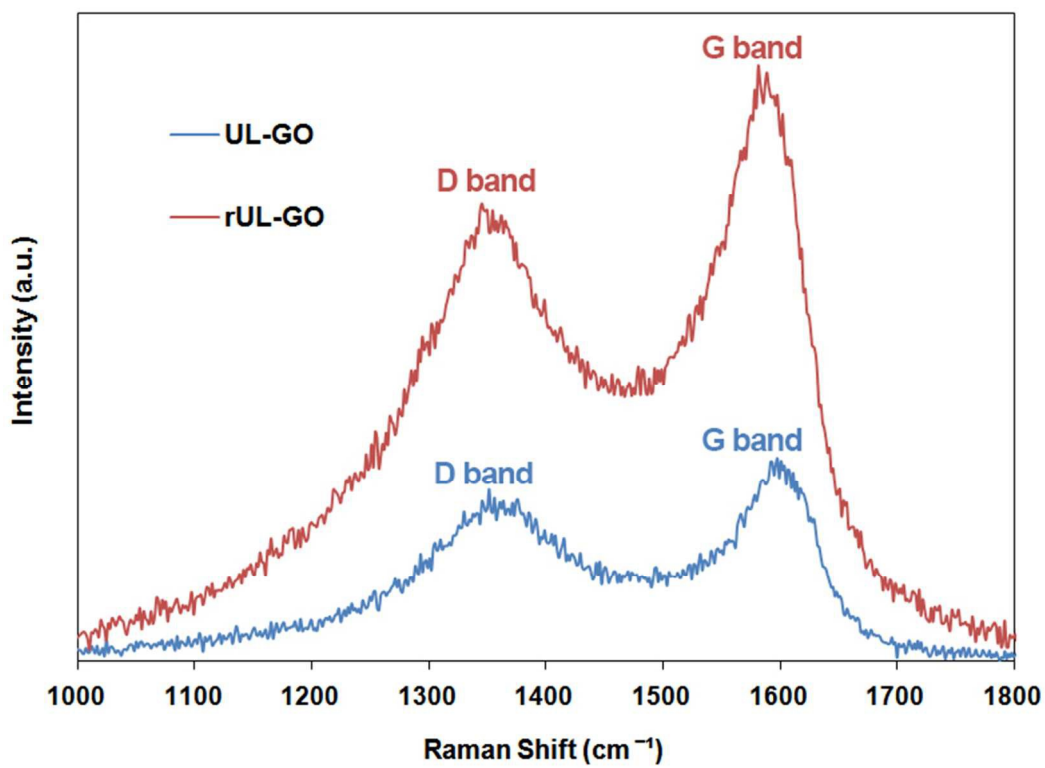Fig. 4 C1s XPS spectra of (a) UL-GO and (b) rUL-GO.

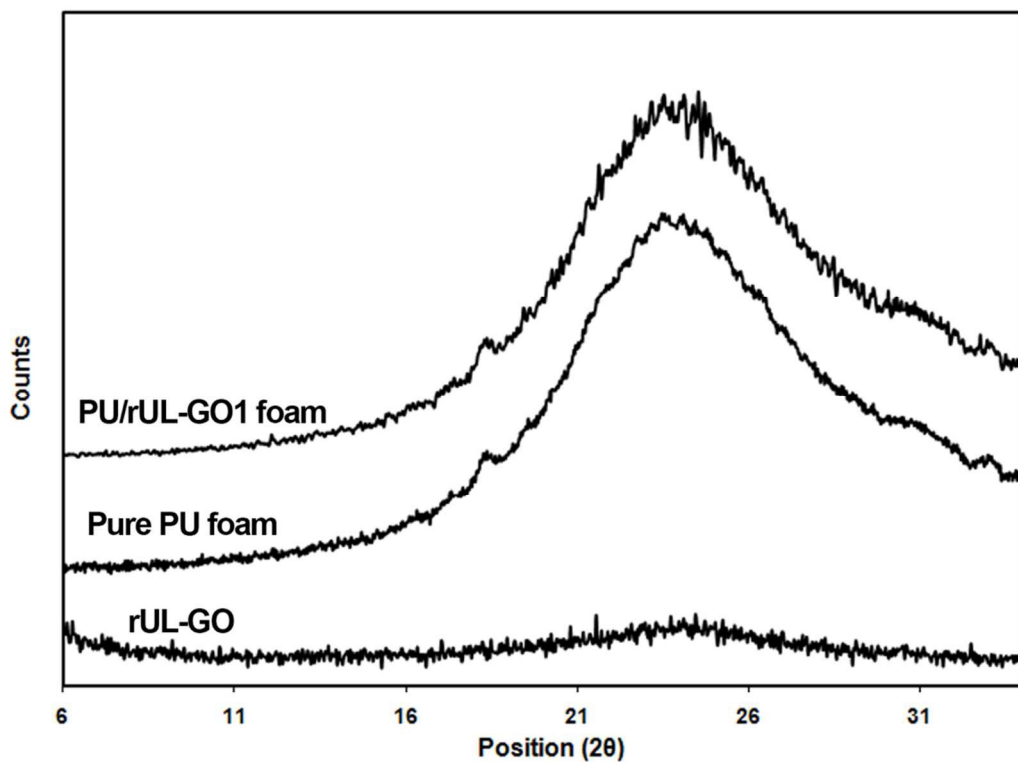Fig. 5 Raman spectra of UL-GO and rUL-GO.

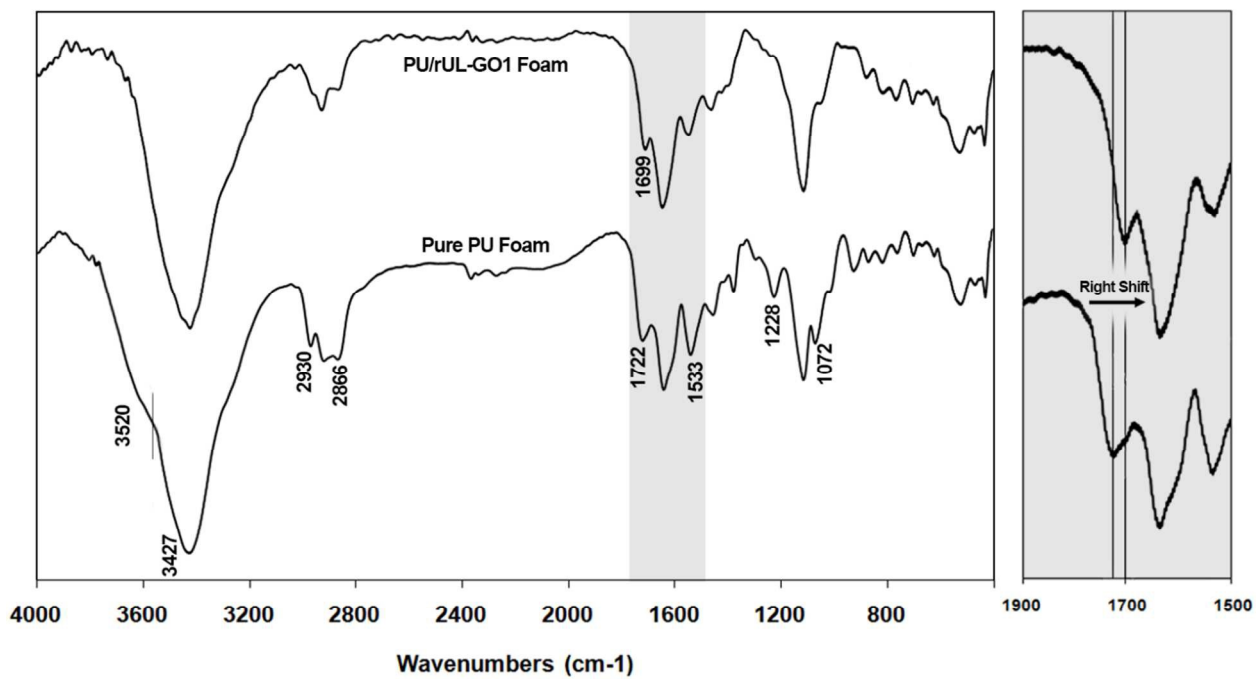Fig .6 XRD patterns of rUL-GO nanosheet, pure PU, and PU/rUL-GO1 foams.

Fig. 7 FTIR spectra of pure PU and PU/rUL-GO1 foams, the highlighted region in original

spectrum is magnified in the right-hand image.
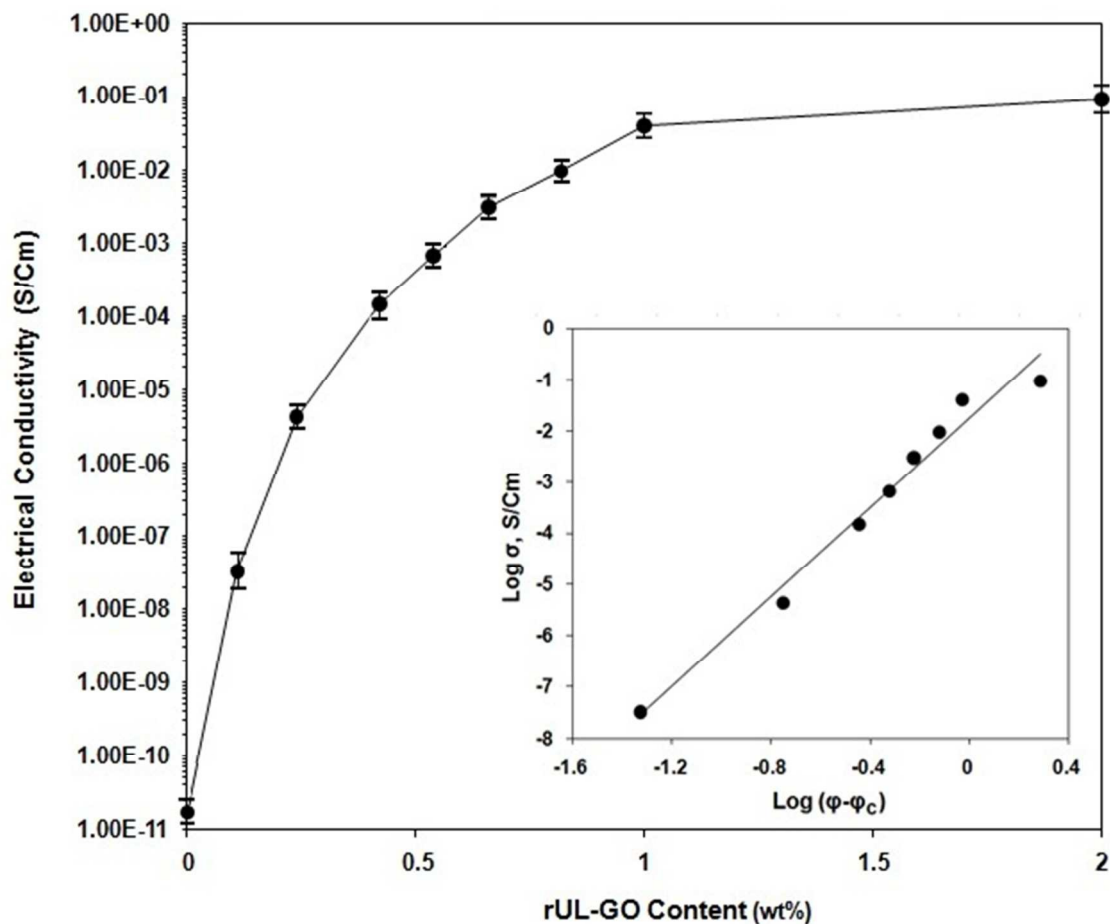
Fig. 8 Electrical conductivity of PU/rUL-GO composite foams as a function of rUL-GO content

(wt %); Inset: log σ plotted against log(φ-φ_c).
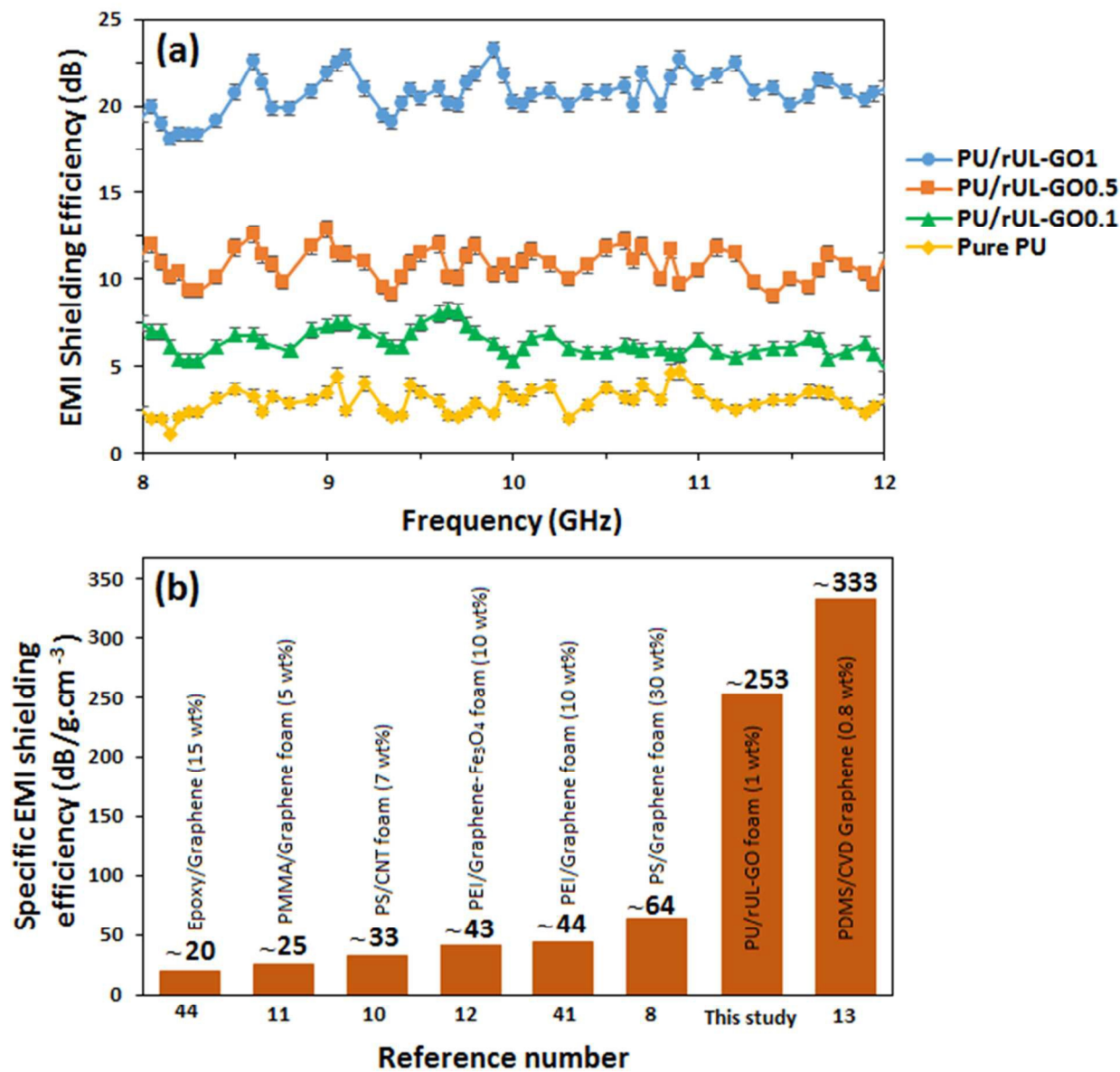
Fig. 9 (a) EMI shielding efficiency of PU/rUL-GO composite foam at different frequency (b) The

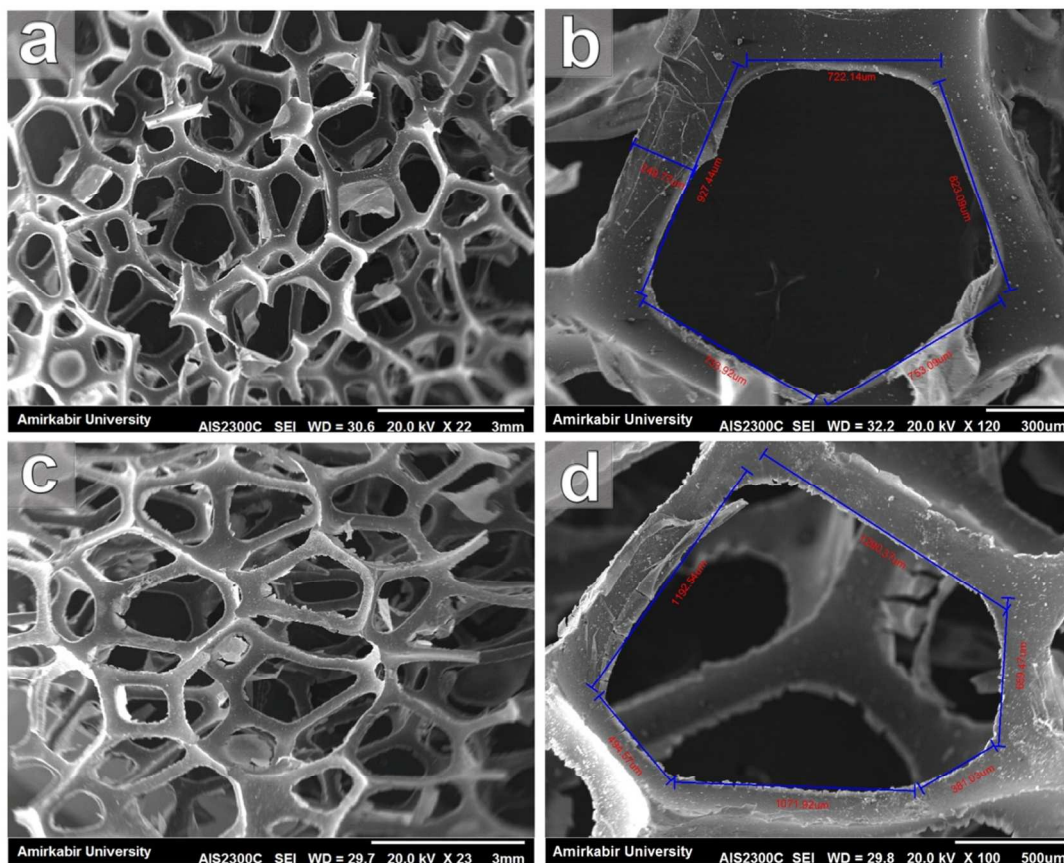comparative of specific EMI shielding efficiency of our data with other reported results.

Fig. 10 SEM micrographs of (a) pure PU, and (c) PU/rUL-GO1 foams. b, and d are the corresponding higher magnification of a and c, respectively.
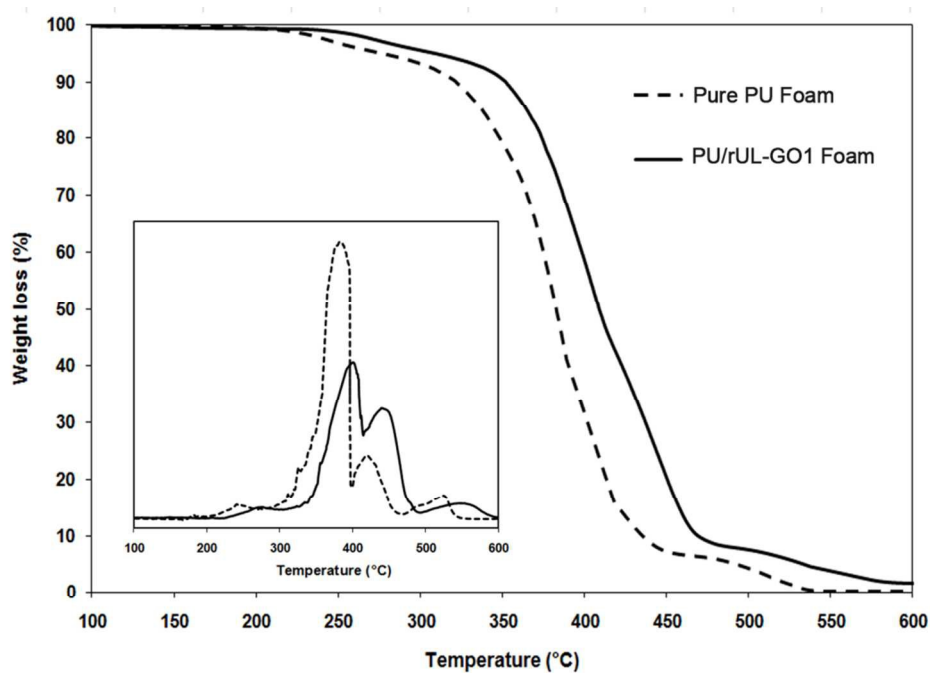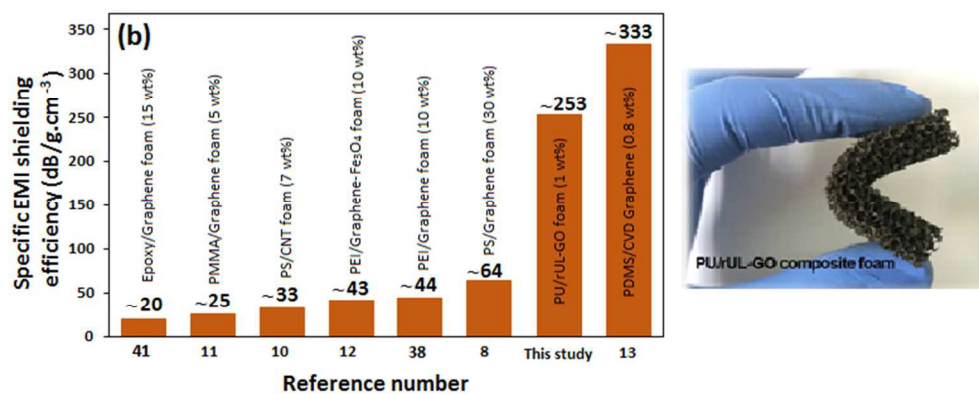
Fig. 11 TGA trace of pure PU and PU/rUL-GO1 foams under nitrogen atmosphere; Inset: DTG

trace.

210x87mm (96 x 96 DPI)